Materials Chemistry and Physics 175 (2016) 172–179

Contents lists available at ScienceDirect

Materials Chemistry and Physics

journal homepage: www.elsevier.com/locate/matchemphys

Nature of active vanadium nanospecies in MCM-41 type catalysts for olefins oxidation

Corina M. Chanquía [a, d, *], Analía L. Cánepa [b, d], Elin L. Winkler [a, d], Enrique Rodríguez-Castellón [c], Sandra G. Casuscelli [b, d], Griselda A. Eimer [b, d]

[a] Centro Atómico Bariloche, Comisión Nacional de Energía Atómica (CAB-CNEA). Av. Bustillo 9500, R8402AGP, San Carlos de Bariloche, Río Negro, Argentina
[b] Centro de Investigación y Tecnología Química (CITeQ), Universidad Tecnológica Nacional, Facultad Regional Córdoba (UTN-FRC), Maestro López esq. Cruz Roja Argentina, Ciudad Universitaria, 5016, Córdoba Capital, Argentina
[c] Departamento de Química Inorgánica, Facultad de Ciencias, Universidad de Málaga (UMA), Av. Cervantes n° 2, 29071, Málaga, Spain
[d] Consejo Nacional de Investigaciones Científicas y Técnicas (CONICET). Avenida Rivadavia 1917, C1033AAJ, Ciudad Autónoma de Buenos Aires, Argentina

HIGHLIGHTS

- Nature of vanadium nanospecies in mesoporous silicates was investigated.
- From hydrothermal sol–gel synthesis, isolated $V^{\delta+}$ sites were mainly generated.
- The coexistence of both vanadium oxidation states V^{4+} and V^{5+} was revealed.
- The catalytic performance was evaluated in α-pinene oxidation with H_2O_2.
- The high catalytic activity is attributed to high dispersion of isolated $V^{\delta+}$ ions.

ARTICLE INFO

Article history:
Received 20 July 2015
Received in revised form
29 February 2016
Accepted 17 March 2016
Available online 24 March 2016

Keywords:
Amorphous materials
Nanostructures
Surface properties
Oxidation

ABSTRACT

A multi-technique physicochemical investigation including UV–Vis-DRS, Raman spectroscopy, XPS, ESR and FTIRS with pyridine adsorption was performed to analyze the nature of different vanadium nanospecies present on MCM-41 type catalysts. By employing a direct hydrothermal synthesis, vanadium species were incorporated into siliceous structure mainly as tetrahedrally coordinated isolated $V^{\delta+}$ ions, which would be located inside the wall and on the wall surface of the mesoporous channels. The coexistence of both vanadium oxidation states V^{4+} and V^{5+} was also revealed. Acidity measurements permitted to infer about the majority presence of Lewis acid sites, which increase with vanadium content. The catalytic performance of these materials was evaluated in the reaction of α-pinene oxidation with H_2O_2. The highest intrinsic activity of the sample with lower V loading was attributed to the high dispersion and efficiency of the isolated $V^{\delta+}$ species that actuate as active sites. A mixture of reaction products arising from competitive processes of epoxidation and allylic oxidation was found.

1. Introduction

In the area of the nanotechnology, one major success has been the development and design of inorganic materials at the nanometric scale with controlled properties suitable to a concrete application [1]. MCM-41, a typical member of the M41S family of mesoporous molecular sieves, had attracted considerable attention as a catalyst support for the processing of bulkier molecules, because of its large surface area (~1000 m^2/g) and uniform pore size distribution with controllable pore size between 20 and 100 Å [2,3]. Numerous studies had been devoted after its discovery to surface modification in order to introduce active metal sites which are necessary for its utility in catalysis [4–6]. MCM-41 has a very flexible framework structure, compared to crystalline zeolites, by allowing the incorporation of various kinds of metals into the silica framework without collapse of its basic structure. Besides Ti-MCM-41 [7–9], other metal containing mesoporous materials that has gained considerable interest is V-MCM-41 [10–12], because of its catalytic potential for selective oxidation of organic compounds,

* Corresponding author. Centro Atómico Bariloche, Comisión Nacional de Energía Atómica, Argentina.
E-mail address: cchanquia@cab.cnea.gov.ar (C.M. Chanquía).

http://dx.doi.org/10.1016/j.matchemphys.2016.03.014
0254-0584/

especially of bulky olefinic compounds, by employing H_2O_2 as oxidant. The functionalization reactions of cyclic olefins as the terpenes are of industrial importance due to the possibility of transforming cheap and readily available substrates, such as α-pinene, to valuable intermediates, among which the oxygenated derivatives are widely used for the synthesis of fragrances, flavors and therapeutic agents.

It is known that the catalytic behavior of these catalysts strongly depends on the nature, content and distribution of the metal species in the matrix, which includes its oxidation state, coordination and dispersion. In this context, one of the main current challenges for materials scientists is to obtain oxides-free mesoporous silicates by maximizing the presence of isolated metal species. Nevertheless, although vanadosilicates are the subject of a greater percentage of the literature reports on mesoporous materials [6,10–24], to date, arguments and discrepancies continue over the assignment of various spectroscopic bands and the nature of the species formed on these mesoporous materials; hence, conclusive evidences are still needed to identify the vanadium species that accounts for the observed catalytic activities.

In a previous work, we reported the hydrothermal synthesis of vanadium-modified mesoporous silicates, its structural and morphological characterization and its catalytic testing in the cyclohexene oxidation by employing H_2O_2 as an oxidant agent [25]. In the present work, we investigated in detail the nature of vanadium nanospecies formed on these mesoporous silicates through a synergistic study of Ultraviolet–visible diffuse reflectance spectroscopy (UV–Vis-DRS), Raman spectroscopy, X-ray photoelectron spectroscopy (XPS) and electron spin resonance (ESR). In addition, the influence of the V content on the distribution of V-nanospecies and the acidic properties of these V-MCM-41 materials are reported, and their catalytic properties are evaluated for the α-pinene oxidation reaction with H_2O_2.

2. Experimental

2.1. Catalysts preparation

The vanadium-containing mesoporous molecular sieves (V-MMS), having various Si/V atomic ratios, were prepared by direct hydrothermal synthesis according to the procedure described by us elsewhere [25]. The color of the final catalysts was white, which turns to yellow when the materials are exposed at atmospheric humidity. The materials were named as V-MMS(x), where x indicates the Si/V molar ratio in the synthesis gel.

2.2. Physicochemical characterization

Ultraviolet–visible diffuse reflectance (UV–Vis-DR) spectra of the materials were performed on samples exposed at atmospheric humidity conditions and after a dehydration treatment in muffle at 773 K during 12 h, by using an Optronics OL 750-427 spectrometer in the wavelength range between 200 and 800 nm. The original spectra obtained for the dehydrated samples have been fitted in bands using multi-peaks fit in OriginPro 8 software. Curve-fitting calculations were useful for determining the location of the bands and their areas; the fitting confidence was $\chi^2 \leq 0.0009$ and $R^2 \geq 0.983$. Raman spectra were taken on a LabRam HR Horiba Raman spectrometer by using 514 nm laser. X-ray photoelectron spectra were collected by using a Physical Electronics PHI 5700 spectrometer with non-monochromatic Mg Kα radiation (300 W, 15 kV, 1253.6 eV) for the analysis of photo-electronic signals of O 1*s*, Si 2*p* and V 2*p* and multichannel detector. Spectra of powdered samples were recorded with the constant pass energy values at 29.35 eV by using a 720 μm diameter analysis area. During data processing of the XPS spectra, binding energy values were referenced to the C 1s peak (284.8 eV) from the adventitious contamination layer. Short acquisition time of 10 min was used to examine C 1*s*, V 2*p* and VLMM XPS regions. The PHI ACCeSS ESCA-V6.0 F software package was used for acquisition and data analysis. A Shirley-type background was subtracted from the signals. Recorded spectra were always fitted by using Gauss-Lorentz curves, in order to determine the binding energy of the different element core levels more accurately. The error in the BE was estimated to be ca. ±0.1 eV. The ESR measurements were performed in an ESP-300 Bruker spectrometer, by operating at a frequency close to 9.4 GHz (X-band) and between 100 and 300 K. To improve the signal-to-noise ratio, all of the spectra presented in this work were measured at 130 K. To evaluate and analyze the strength and type of the acid sites, FTIR spectral measurements of pyridine adsorption on the samples were performed on a JASCO 5300 spectrometer, equipped with a DTGS detector. The measurement range and resolution were 4600–400 and 4 cm^{-1}, respectively. Self-supporting wafers for each sample (~20 mg/cm^2) were prepared, placed in a thermostatized cell with CaF_2 windows connected to a vacuum line and evacuated for 8 h at 673 K. The background spectrum was recorded first after cooling the sample to room temperature. Afterwards, the solid wafer was exposed to pyridine vapors at room temperature and allowed to saturate for 20 min. The IR spectrum for each sample was obtained after pyridine desorption by evacuation for 1 h at 373 K and 473 K. The difference spectrum was obtained finally by subtracting the background spectrum recorded previously.

2.3. Catalytic performance

The α-pinene oxidation reaction was carried out in a glass reactor with a magnetic stirrer, immersed in a thermally controlled bath at 343 K. Typically, the reaction mixture consists of 6.14 mmol of α-pinene, 1.54 mmol of H_2O_2 35%, 92.19 mmol of acetonitrile and 54 mg of catalyst. Reaction progress was followed taking samples during reaction through sealed septa by means of a syringe. Liquid samples were filtered and analyzed by gas chromatography using a capillary column (crosslinked methyl–silicone gum) connected to a FID detector. Reaction products were identified by mass spectrometry in a Shimadzu GCMS-QP 5050 with HP-5 capillary column. The α-pinene conversion was defined as the ratio of converted species to initial concentration and the selectivity as (mol product/mol total products) x 100. The turnover number (TON) was defined as moles of olefin converted/mol of metal in the catalyst. Finally, the total conversion of H_2O_2 was measured by iodometric titration and H_2O_2 efficiency was calculated as the percentage of this reactive converted to total oxidized products.

3. Results and discussion

Table 1 summarizes the structural and morphological properties of the V-MMS synthesized with different V contents, reported by us elsewhere [25]. All materials exhibited MCM-41 type mesoporous structure, high surface areas between 900 and 1400 m^2/g and a narrow pore size distribution around to 2.4 nm. Specific surface area values of V-MMS(60) and V-MMS(240) samples are very similar (~1375 m^2/g, respectively) possibly due to their very low vanadium content (<0.15 wt %). However, the V-MMS(20) sample, synthesized with the highest content of vanadium, shows the lower surface area (934 m^2/g) probably due to the partial blocking of mesopores by V-nanoclusters and/or nano-oxides (<5 nm) [25].

The UV–Vis-DR spectra were recorded in order to understand the coordination environment of V-nanospecies in these MCM-41 type structures. These spectra for the samples previously

dehydrated in muffle at 773 K during 12 h are showed in Fig. 1. The original spectra can be decomposed into four contributions which can be assigned to different vanadium species. It is known that the (CT) charge transfer bands are strongly influenced by the local structure of vanadium sites and also isolated vanadium species generally give rise to CT transitions in a higher energy region than polymeric species. Thus, the two first bands at 260 and 300 nm arise from O^{2-} to V^{5+} charge-transfer (LTMC) assigned to electron transfers $(\pi)t_2 \rightarrow (d)e$ and $(\pi)t_1 \rightarrow (d)e$, respectively, for central V ions tetrahedrally coordinated with oxygen ligands [26–28]. Although many authors have reported that these double bands are attributed to T_d-V^{5+} inside the walls and on the wall surfaces [14,29], respectively, other researchers have suggested that the CT transition for the V^{4+} is also expected between 250 and 285 nm [30,31]. It should be noted here that the presence of V^{4+} in our samples was detected by XPS and ESR (see below). Therefore, on the basis of the above information and our observations, we could suggest, a priori, that at least two isolated $V^{\delta+}$ species coordinated with the lattice oxygen in a tetrahedral environment, could be present. In addition, the bands at 320 and 380 nm, associated with CT transitions of O to V corresponding to higher coordinated $V^{\delta+}$ ions in an octahedral environment [29,30], could be giving account for the presence of oligonuclear $(V^{\delta+}\cdots O^{\delta-}\cdots V^{\delta+})_n$ nano-clusters arising from an incipient oligomerization of V species [27,30,32]. Finally, in the visible region no additional absorption bands, especially near 600 nm corresponding to d–d transitions of vanadyl VO^{2+} ions, are seen. Generally, these transitions are masked by more intense CT transitions. In fact, since the d–d transition intensities of vanadyl VO^{2+} ions are generally 10–30 times weaker than those of the CT transitions [14,30], such absorption is apparently undetected by UV–Vis-DR, despite V^{4+} ions were detected by XPS in our samples.

To elucidate the change of vanadium centers during hydration/dehydration, we have studied the UV–Vis-DR spectra changes (Fig. 2) for all the samples exposed at atmospheric humidity conditions (a) and after a dehydration treatment in heating muffle at 773 K during 12 h (b). As it can be seen, the spectra of the samples exposed at atmospheric humidity appear widened toward higher wavelengths. Thus, the intense bands at about 300 and 400 nm in the spectra (a), corresponding to $V^{\delta+}$ species with square pyramidal and distorted octahedral structures, respectively, can be associated with tetrahedral $V^{\delta+}$ coordinating water molecules to become five- and six-coordinated [14,30]. Then, such spectral changes indicate that the $V^{\delta+}$ coordination increases to form square pyramidal and then octahedral geometries by contacting with water molecules under atmospheric humidity conditions. Upon the dehydration treatment, the samples previously yellow became white and the spectra are narrowed towards lower wavelength according to the presence of tetrahedral coordinated and colorless $V^{\delta+}$ ions. After a new exposure of these samples to atmospheric humidity conditions the color changes rapidly to yellow, indicating the additional coordination of water molecules to the $V^{\delta+}$ ions as reflected by the broadening of the spectra toward higher wavelengths. Repeated dehydrations and hydrations show that both the color and UV–Vis-DR spectral changes are reversible. On the other hand, it should be noted that although all the UV–Vis-DR spectra are broadening upon atmospheric humidity conditions, the intensity of the absorption at the lowest wavelength corresponding to tetrahedral $V^{\delta+}$ species are not practically modified. This suggests the presence of some tetrahedral $V^{\delta+}$ species, probably located inside the framework, inaccessible to additional coordination by water. Therefore, these observations permit us to confirm the existence of two isolated vanadium species into the framework: ones, inaccessible, incorporated inside the wall and others located on the wall surface of the mesoporous channels, to which water molecules can easily access and increase its coordination environment.

Table 2 shows an estimation of the percentage of the different V species in the dehydrated samples. Distribution of these V species depends on the quantity of vanadium in the initial gel. From UV–Vis-DR data, most of the vanadium is incorporated into the structure as isolated $V^{\delta+}$ species tetrahedrally coordinated. Then, as it can be deduced, the relative proportion of these tetrahedral V species, that are located in the wall surface and accessible to additional coordination by water, is seen increased with increasing vanadium content. This feature could give account for the strong increase in the absorptions at higher wavelength in the case of the hydrated samples with higher V content. Meanwhile, the increase of V content would be causing an increase in the degree of polymerization of the V species giving rise to the formation of the $(V^{\delta+}\cdots O^{\delta-}\cdots V^{\delta+})_n$ nanoclusters. These species would be increasing its size when the V content increases, judging by the appearance of an absorption band at higher wavelength (380 nm) for the dehydrated V-MMS(20) sample. In Table 2, it is also shown a marked increase in the Si/V molar ratio of the final solids with respect to the same ratio in the initial synthesis gel. This possibly indicates that only a small proportion of the vanadium initially introduced into the synthesis gel is retained by the siliceous structure.

Raman spectroscopy was employed in order to complement the information already obtained by UV–Vis-RD. Fig. 3 shows the Raman spectra of calcined V-MMS(x) samples and the pure siliceous Si-MMS. The introduction of vanadium species in the MCM-41 structure gives Raman bands at 269, 335, 920 and 1018 cm^{-1}. Thus, Raman band of 1018 cm^{-1} corresponds to the stretching frequency of a terminal of V=O group bonded to the silicate MCM-41 [6,33]. In addition, the Raman band at 269 cm^{-1} can be ascribed to the V–O–V bending mode and the bands centered around 335 and 920 cm^{-1} may correlate with the V–O–V stretching vibrations [6,33]; these bands are increased with increasing content of V. Finally, the absence of typical bands to 995, 703 and 530 cm^{-1} implies that no crystalline V_2O_5 is formed in the samples, which is in accordance with XRD [25] and UV–Vis-RD results. This suggests

Table 1
Structural parameters of the V-MMS synthesized with different V contents.

Sample	Si/V[a]	$d_{(100)}$[b] (nm)	a_0[c] (nm)	D_{BJH}[d] (nm)	t_w[e] (nm)	Mesop. Vol. (cm^3/g STP)[f]	A_{BET}[g] (m^2/g)
V-MMS(20)	20	3.96	4.57	2.65	1.92	0.36	934
V-MMS(60)	60	3.52	4.06	2.25	1.81	1.03	1380
V-MMS(240)	240	3.30	3.81	2.45	1.36	1.06	1370

[a] Molar ratio in the initial gel.
[b] interplanar spacing (100).
[c] lattice parameter.
[d] BJH pore diameter.
[e] wall thickness calculated by a_0 - D_p.
[f] pore volume;.
[g] BET specific surface area.

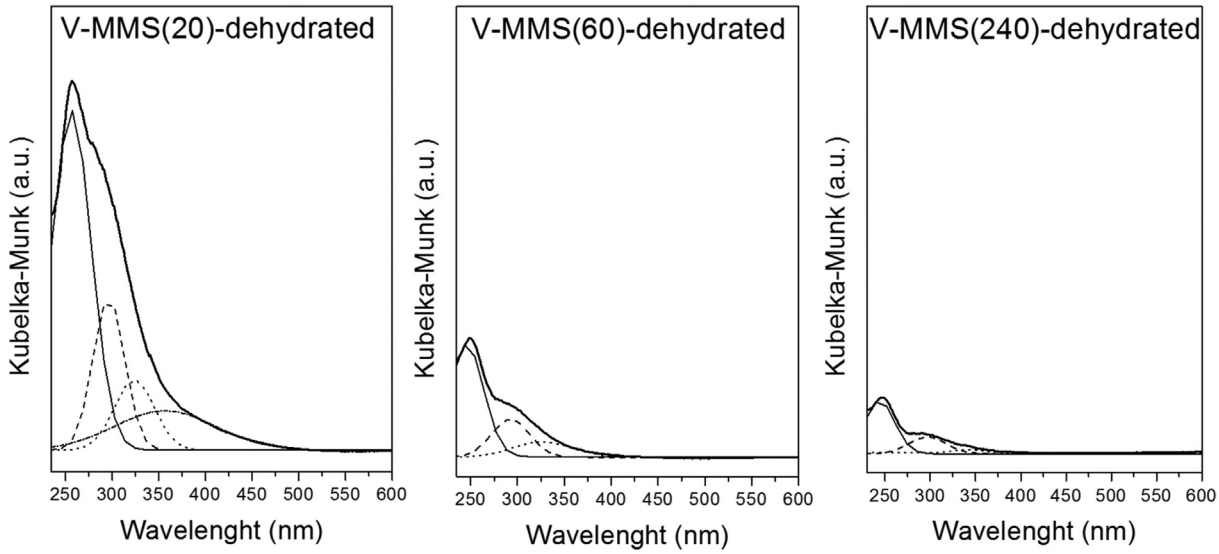

Fig. 1. Deconvoluted UV–Vis-DR spectra of dehydrated V-MMS(x) (solid lines: isolated $V^{\delta+}$ inside the wall, dashed lines: isolated $V^{\delta+}$ on the wall surface, dotted lines: $(V^{\delta+}\cdots O^{\delta-}\cdots V^{\delta+})_n$ nano-clusters.

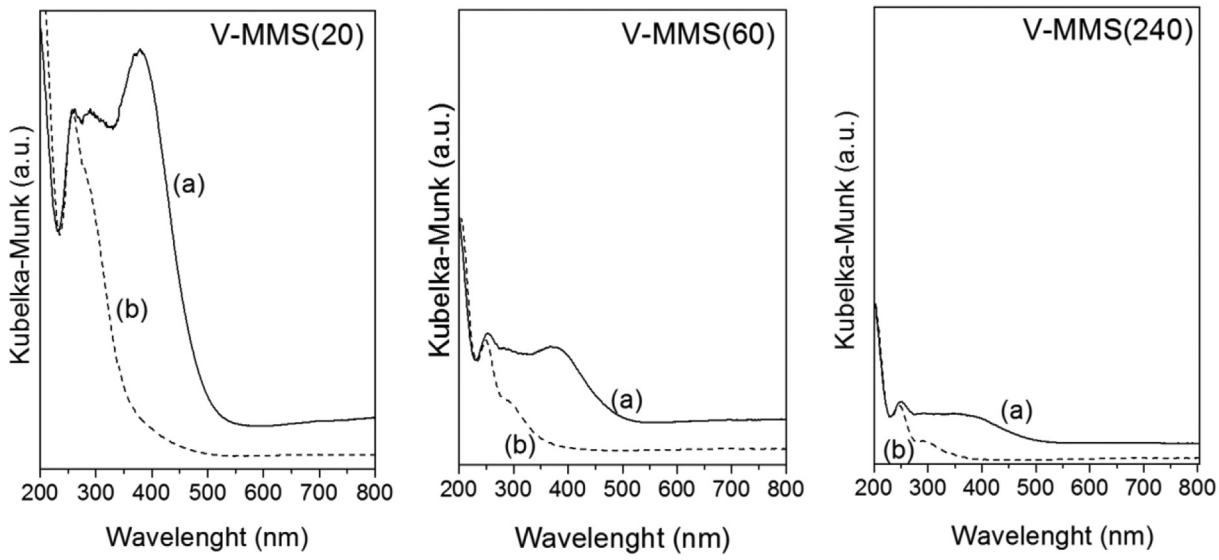

Fig. 2. UV–Vis-DR spectra of V-MMS(x) recorded before (a) and after (b) a dehydration treatment at 773 K during 12 h.

that the vanadium species in V-MMS(x) are isolated or, at least, highly dispersed on the surface.

The ESR spectra collected at 130 K of V-MMS materials with different vanadium contents are shown in Fig. 4. This figure also includes, as reference, the ESR spectra of the vanadyl sulfate (V^{4+}, 3 d^1) source. All the spectra were normalized by the atomic concentration of vanadium. This figure evidences a marked decrease of the ESR signal for the catalysts in comparison with the vanadium

Table 2
Chemical composition and vanadium species relative distribution in V-MMS modified with different V contents.

Sample	V Content[a] [wt. %]	Si/V[a]	Distribution of V-nanospecies							
			$V^{\delta+}$ inside wall		$V^{\delta+}$ on wall surface		$V^{\delta+}$ in extraframework clusters			
			~250 nm		~290 nm		~320 nm		~380 nm	
			area %	wt. %	area %	wt. %	area %	wt. %	area %	wt. %
V-MMS(20)	1.210	71.5	54	0.66	19	0.230	11	0.130	16	0.19
V-MMS(60)	0.140	676.8	62	0.087	23	0.032	15	0.021	–	–
V-MMS(240)	0.035	2416.3	71	0.025	15	0.005	13	0.005	–	–

[a] In the final solid.

source. This result could indicate that many of the V^{4+} ions are oxidized during the V-MMS catalyst synthesis. The oxidation of V^{4+} to V^{5+} (3 d^0) probably occurs during the high pH hydrothermal synthesis and/or the subsequent calcination treatment [34–36]. Notice that the ESR signal diminished when the concentration of vanadium was reduced and for the most diluted V-MMS(240) sample the ESR absorption is barely distinguished. The features of the V-MMS spectra are similar for the different vanadium concentrations and allow assigning the ESR lines to the resonance of well diluted V^{4+} ions located in sites with axial symmetry. The powder spectrum, shown in Fig. 5, can be described by the following spin Hamiltonian, H, that includes the Zeeman interaction of the single unpaired electron, S = 1/2, of the V^{4+} with the external magnetic field and the hyperfine interaction of the electronic spin with the nuclear spin I = 7/2 of the ^{51}V, of natural abundance of 99,76%:

$$H = H_z + H_h = \sum_i \{\mu_B S_i.g.H_o + S_i.A.I_i\}$$

where μ_B is the Bohr magneton and the parameters g and A are 2nd order tensors. For axial symmetry, the principal values of the g and A tensors are $g_\perp = g_x = g_y$, $g_{//} = g_z$ and $A_\perp = A_x = A_y$, $A_{//} = A_z$. The powder spectrum is obtained from the sum of the spectra corresponding to crystallites oriented in all of the possible space directions. From Fig. 5 two groups of peaks are clearly observed centered in $H_{//}$and $H_\perp$; from these values, $g_{//}$= 1.931 (5) and $g_\perp$ = 1.986 (5) were obtained. This figure also indicates the splitting of the absorption resonance due to the hyperfine interaction, which allows us to determine the $A_{//}$ = 204 (2) Oe and $A_\perp$ = 77 (2) Oe.

In order to obtain more details about the nature of the vanadium nano-species on V-MMS, measurements of X-ray photoelectron spectroscopy were carried out. The V $2p_{3/2}$ core level spectra of the V-MMS samples prepared with different V loadings after 10 min of irradiation are shown in Fig. 6. As it is possible to observe from the curve-fitted spectra, the V $2p_{3/2}$ region shows two peaks at ~515.6 eV and ~517.1, assigned to V^{4+} and V^{5+} ions, respectively [34–37]. This is according to some authors that state that a partial oxidation of V^{4+} species, present in the synthesis gel, takes place during calcination. Thus, XPS in combination with ESR data

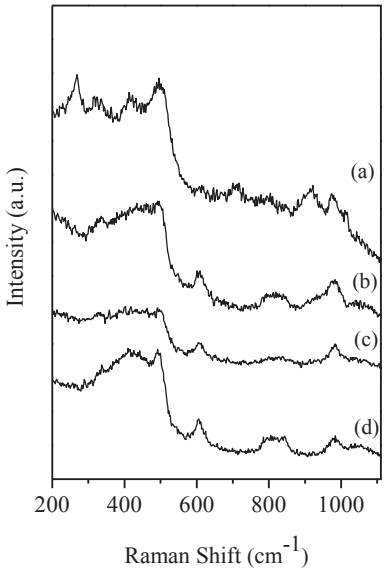

Fig. 3. Raman spectra of (a) V-MMS(20), (b) V-MMS(60), (c) V-MMS(240) and (d) Si-MMS.

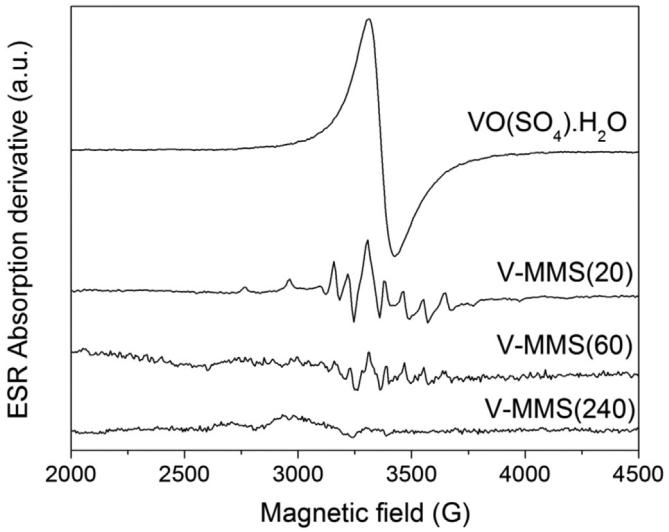

Fig. 4. ESR spectra collected at 130 K of V-MMS(x). It is also includes the spectrum of the vanadyl sulfate (V^{4+}, d^1) source. Measurements were performed on samples under atmospheric humidity conditions and all the spectra were normalized by the atomic concentration of vanadium.

confirms the presence of both +4 and + 5 oxidation states of vanadium. It is noteworthy that the V-MMS(240) sample did not show XPS signal in the V $2p_{3/2}$ region. However taking into account the low percentage of vanadium on this sample in conjunction with the detection limit estimated for the XPS analysis (~0.1%) is not surprising the lack of a discernible V peak. Table 3 summarizes the binding energy values and surface Si/V and O/Si atomic ratios as well as the quantification of both species V^{4+} and V^{5+} considering the V $2p_{3/2}$ region, for the samples modified with different vanadium contents. The O 1*s* peak position at ~532.8 eV is as expected for silica. Likewise, 103.6 eV for the Si 2*p* peak is in agreement with SiO_2-type material [34]. The position of these latter peaks for all the V-MMS samples has not substantially changed. On the other hand, it can be seen that the V-MMS(20) sample shows a lower surface Si/V atomic ratio than the V-MMS(60) sample, evidencing the higher percentage of vanadium species on the external surface of the microspheres when the V content is increased.

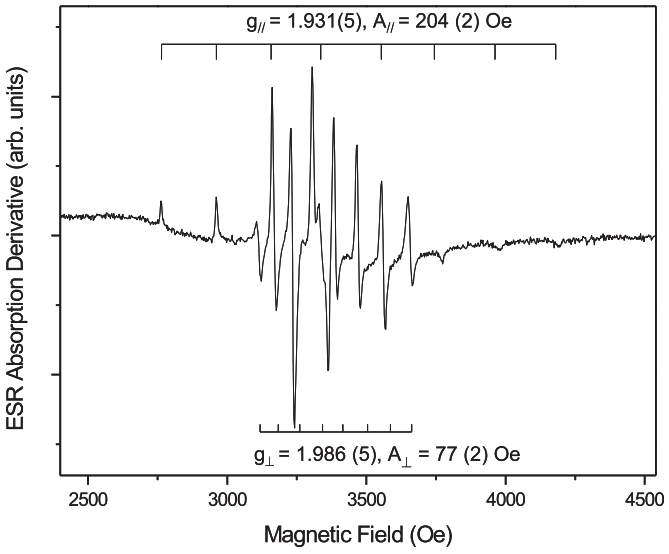

Fig. 5. ESR spectra corresponding to the V-MMS(20) measured at 130 K.

The chemisorption of pyridine followed by IR studies is usually a useful probe to detect the presence and nature of acid sites on a catalyst [8]. Information on the strength of Lewis and Brønsted acid sites can be obtained from pyridine thermodesorption. Fig. 7 shows FT-IR spectra of the V-MMS(x) samples, recorded after the adsorption of pyridine and subsequent evacuation at 100 and 200 °C, Fig. 7 (a) and (b) respectively. All the samples show bands corresponding to hydrogen bonded pyridine at 1447 cm^{-1} and 1599 cm^{-1} [38–43]. As it can be observed, a band at 1609 cm^{-1}, corresponding to pyridine coordinately bonded to Lewis acid sites is increased proportionally according to the amount of vanadium incorporated into the material [38–45]. Moreover, an increase in the IR absorption band present at 1447 cm^{-1} with growing vanadium content could be interpreted in terms of the overlapping of both the hydrogen-bonded pyridine band (1447 cm^{-1}) and a band attributed to a Lewis-type adduct which frequently appears at 1450 cm^{-1} [41]. Moreover, a slight band at 1577 cm^{-1} due to pyridine coordinated to weak Lewis sites was also observed for the V-MMS(20) and V-MMS(60) samples [8]. Taking into account that sample wafers had approximately the same weight and surface density, a semi-quantitative estimation allowed us to suggest that the incorporation of V into the silica framework generates Lewis acid sites on the surface which increase with increasing vanadium content. These sites can be mainly attributed to the presence of coordinatively unsaturated surface $V^{\delta+}$ sites. On the other hand, the catalysts synthesized with the higher V contents exhibit a band at ~1545 cm^{-1} which is remarkably more intense for the V-MMS(20) sample. Moreover, a band at 1639 cm^{-1} can be clearly observed for this sample with the highest vanadium. These latter bands distinctively identify the pyridinium ion [43,46–48]. Thus, we can assume that the incorporation of vanadium gives rise to a small amount of Bronsted acid sites on the surface [43,48–50]. However, under evacuation at 200 °C these bands tend to disappear, indicating that these Bronsted sites are of a weak character. In addition, a band corresponding to vibration of pyridine associated with both, Lewis and Bronsted acid sites, was observed at 1490 cm^{-1}. On the other hand, taking into account the relative intensity of the bands associated with the Lewis and Bronsted acid sites, the Lewis acidity resulted more important. Moreover, while the band at 1599 disappears upon evacuation at 200 °C, indicating a weak interaction between pyridine and the SiOH groups of the structure, the presence of the band at 1447 cm^{-1} at this temperature provides clear evidence that the same has a contribution from Lewis acid sites which are strong enough to retain the pyridine molecules until 200 °C. After desorption above 200 °C, all the bands completely disappeared indicating the medium acid strength of these materials.

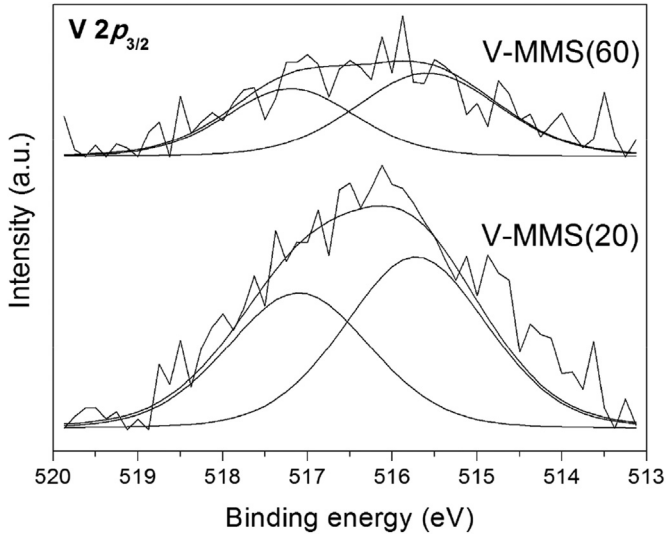

Fig. 6. V $2p_{3/2}$ core level photoelectron profile of V-MMS(x). Measurements were performed on samples under atmospheric humidity conditions.

Table 3
BE values (in eV) and surface Si/V and O/Si atomic ratios in V-MMS modified with different V contents.

Sample	O 1*s*	Si 2*p*	V $2p_{3/2}$	Si/V	O/Si
V-MMS(20)	533.0	103.8	517.20 (42%) 515.60 (58%)	217.33	2
V-MMS(60)	533.0	103.6	517.10 (44%) 515.70 (56%)	366.78	2
V-MMS(240)	532.5	103.3	(nd)[a] (nd)[a]	∞	2.37

[a] no discernible.

Fig. 7 also shows the IR spectra of the samples in the hydroxyl range before pyridine adsorption. Only a very intense band at 3740 cm^{-1}, corresponding to the υ(O–H) stretching vibrations of isolated terminal hydroxyl groups, can be clearly observed [38,40,48]. Moreover, a smooth shoulder around 3550 cm^{-1} allows us to infer about a possible interaction between vicinal OH groups, as Si–OH, V–OH and H–OH [34,37,51].

The catalysts synthesized with different V contents were tested in the reaction of α-pinene oxidation with H_2O_2 at 343 K. As it is shown in Table 4 the conversion of α-pinene is in the range 10–13 mol %, which represents about 40–52% of maximin. The higher activity of the samples with lower V content (V-MMS(60) and V-MMS(240)) is thought to be due to the good dispersion of active sites, originating from isolated vanadium species in a tetrahedral coordination in the framework [25]. Besides, the slight increase observed in the conversion when the Si/V molar ratio of the samples is changed from 240 to 60 could be related to the increase in the relative proportion of accessible tetrahedral V species located in the wall surface. Meanwhile, the reason for the lowest catalytic activity over the V-MMS(20) sample can be associated to the presence of the $(V^{\delta+}\cdots O^{\delta-}\cdots V^{\delta+})_n$ nanoclusters (observed by UV–Vis-DR) arising from an increase in the degree of polymerization of the V species. On the other hand, the H_2O_2 conversion increases with the V content in the samples, while its efficiency shows an opposite trend (see Table 4). This behavior could be also attributed to the higher proportion of vanadium species as extra-framework nanoclusters which would be responsible for the decomposition of peroxide to water, resulting in a lower α-pinene conversion. Besides, these species, placed both inside the channels and on the external surface, could diminish and block the accessibility to the active sites (isolated V ions) causing a further decrease of the catalytic activity [25]. In addition, in order to compare the intrinsic catalytic activity of the different catalysts, the turnover numbers (TON) are also given in Table 4. They decrease strongly with increasing V content, which could infer that much of the vanadium incorporated is not effectively used for the catalytic oxidation. Meanwhile, the higher intrinsic activity for the catalyst with lower metal content would be giving account for the high dispersion and efficiency of the active sites incorporated on this material. In addition, blank experiments, without any catalyst or with V-free silica were carried out. The reaction did not proceed in the absence of the catalyst and the α-pinene conversion on pure silica Si-MMS was very low (<1 mol %). Hence the enhanced conversion observed over V-MMS(x) confirms the role of V ions in the present reaction.

Finally, the selectivity to the different products observed for 7 h

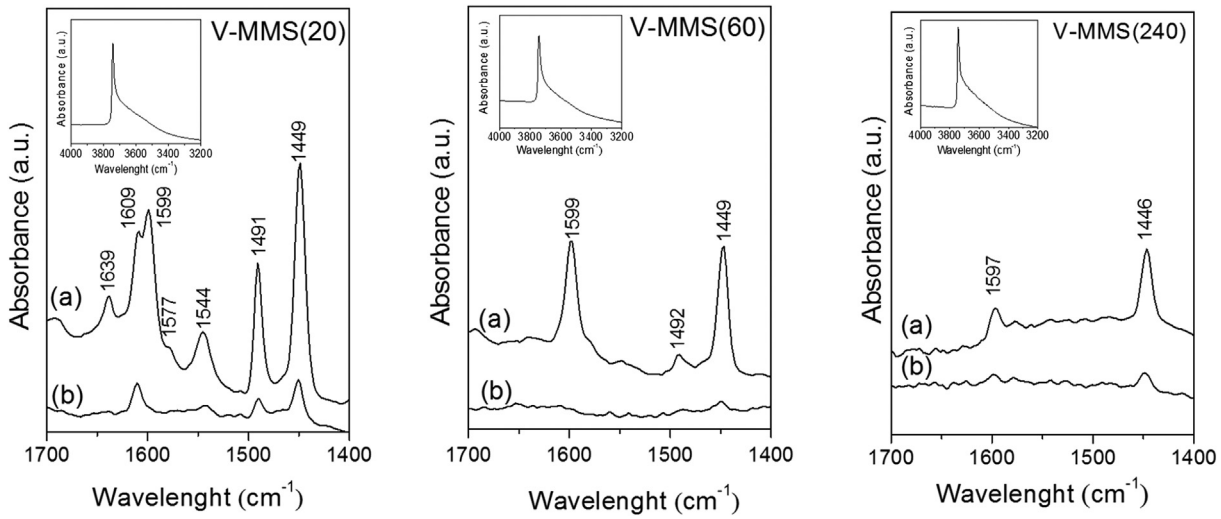

Fig. 7. FTIR of pyridine adsorbed on V-MMS(x), after desorption at 373 K (a) and 473 K (b). Inserted in spectrum of each sample is the region of OH before pyridine adsorption.

Table 4
α-pinene oxidation with H_2O_2 on V-MMS catalysts. Reaction conditions: α-pinene/H_2O_2 molar ratio = 3.92; temperature = 343 K; reaction time = 7 h.

Si/V	% wt.	α-pinene conversion (mol %)	TON[a]	H_2O_2		Selectivity[c] (mol %)						
				Conversion (mol %)	Efficiency[b] (mol %)	(1)	(2)	(3)	(4)	(5)	(6)	Over-oxidation products
20	1.21	10.0	42.9	91.3	38.3	2.1	33.7	12.2	21.8	4.1	9.1	16.8
60	0.14	12.8	500.0	84.5	53.2	4.7	13.4	15.9	36.3	11.4	7.8	10.5
240	0.035	11.4	1888.6	79.7	57.2	2.7	24.1	3.7	5.3	14.1	46.0	4.2

[a] TON: moles of olefin converted/mol of vanadium in the catalyst.
[b] H_2O_2 efficiency: moles of products formed (1–6+ over-oxidation products)/mol of H_2O_2 reacted.
[c] (1)α-pinene oxide, (2) campholenic aldehyde, (3)1,2 pinanediol, (4) trans sobrerol, (5) verbenol, (6) verbenone.

reaction is also shown in Table 4 for all the synthesized catalysts. Often, epoxidation and allylic oxidation are competitive processes in the oxidation of cyclic olefins and frequently both processes occur simultaneously giving a mixture of reaction products. Thus, according to GC–MS analyses, our products mixture is composed of molecules arising from the oxidation of both double bond (α-pinene oxide, campholenic aldehyde, 1,2 pinanediol, trans sobrerol) and allylic C–H bond (verbenol and verbenone). In addition, over-oxidation products, increasing with the higher V contents, are also observed. Probably, the presence of $(V^{\delta+}\cdots O^{\delta-}\cdots V^{\delta+})_n$ nanoclusters of increased size, mainly observed for the V-MMS(20) sample, is favoring the consecutive reactions of over-oxidation [52].

4. Conclusions

By employing a direct hydrothermal synthesis, vanadium species are incorporated into the siliceous framework mainly as isolated $V^{\delta+}$ cations in tetrahedral coordination with the lattice oxygen. The presence of oligonuclear $(V^{\delta+}\cdots O^{\delta-}\cdots V^{\delta+})_n$ nanoclusters, arising from an incipient oligomerization of V species and whose size seems to be increased with the V content increasing, could also be identified. The coexistence of both V oxidation states 4 + and 5+ (δ+) in the different nanospecies could be also inferred. The incorporation of isolated $V^{\delta+}$ species coordinated to framework oxygen atoms mainly generated Lewis acid sites, which increase with V content. These V-MCM-41 catalysts showed good activity for the α-pinene oxidation with H_2O_2 as oxidant. The higher intrinsic activity of the catalyst with lower metal content would be giving account for the high dispersion and efficiency of the active sites (isolated $V^{\delta+}$ species incorporated into the framework). On the other hand, the higher proportion of vanadium species as extra-framework nanoclusters, in the samples with higher V content, could cause the decomposition of peroxide to water, resulting in lower H_2O_2 efficiency and α-pinene conversion.

Acknowledgments

C.M.C., A.L.C., E.L.W. S.G.C. and G.A.E. are CONICET Researchers. This work was supported by CONICET, UTN-FRC and CNEA of Argentina, and UMA of Spain.

References

[1] G. Soller-Illia, C. Sanchez, B. Lebeau, J. Patarin, Chem. Rev. 102 (2002) 4093–4138.
[2] C. Kresge, M. Leonowicz, W. Roth, J. Vartuli, J. Beck, Nature 359 (1992) 710–712.
[3] J. Beck, J. Vartuli, W. Roth, M. Leonowicz, C. Kresge, K. Schmitt, C. Chu, D. Olson, E. Sheppard, S. McCullen, J. Higgins, J. Schlenker, J. Am. Chem. Soc. 114 (1992) 10834–10843.
[4] A. Sayari, Chem. Mater 8 (1996) 1840–1852.
[5] A. Corma, Chem. Rev. 97 (1997) 2373–2419.
[6] S. Shylesh, A. Singh, J. Catal. 233 (2005) 359–371.
[7] G. Eimer, S. Casuscelli, G. Ghione, M. Crivello, E. Herrero, Appl. Catal. A 298 (2006) 232–242.
[8] G. Eimer, S. Casuscelli, C. Chanquía, V. Elías, M. Crivello, E. Herrero, Catal. Today 133–135 (2008) 639–646.
[9] G. Eimer, I. Díaz, E. Sastre, S. Casuscelli, M. Crivello, E. Herrero, J. Perez-Pariente, Appl. Catal. A 343 (2008) 77–85.
[10] K. Reddy, I. Moudrakovski, A. Sayari, J. Chem. Soc. Chem. Commun. (1994) 1059–1060.
[11] M. Mathieu, P. Vander Voort, B. Weckhuysen, R. Rao, G. Catana, R. Schoonheydt, E. Vansant, J. Phys. Chem. B 105 (2001) 3393–3399.
[12] J. Reddy, P. Liu, A. Sayari, Appl. Catal. A 148 (1996) 7–21.
[13] S. Gontier, A. Tuel, Micropor. Mater 5 (1995) 161–171.
[14] Z. Luan, J. Xu, H. He, J. Klinowski, L. Kevan, J. Phys. Chem. 100 (1996) 19595–19602.

[15] S. Lim, G. Haller, J. Phys. Chem. B 106 (2002) 8437–8448.
[16] Y. Gucbilmeza, T. Dogua, S. Balci, Catal. Today 100 (2005) 473–477.
[17] J. Xu, W. Chu, S. Luo, J. Mol. Catal. A Chem. 256 (2006) 48–56.
[18] X. Guo, N. Xue, S. Liu, X. Guo, W. Ding, W. Hou, Micropor. Mesopor. Mat. 106 (2007) 246–255.
[19] V. Parvulescu, C. Anastasescu, B. Su, J. Mol, Catal. A Chem. 198 (2003) 249–261.
[20] J. Santamaría-González, J. Luque-Zambrana, J. Mérida-Robles, P. Maireles-Torres, E. Rodríguez-Castellón, A. Jiménez-López, Catal. Lett. 68 (2000) 67–73.
[21] Y. Yang, S. Lim, C. Wang, D. Harding, G. Haller, Micropor. Mesopor. Mat. 67 (2004) 245–257.
[22] J. Herrera, J. Hun Kwak, J. Zhi Hu, Y. Wang, C. Peden, Top. Catal 39 (3–4) (2006) 245–255.
[23] Y. Wang, Q. Zhang, Y. Ohishi, T. Shishido, K. Takehira, Catal. Lett. 72 (3–4) (2001) 215–219.
[24] Y. Hu, N. Wada, K. Tsujimaru, M. Anpo, Catal. Today 120 (2007) 139–144.
[25] C. Chanquía, A. Cánepa, K. Sapag, P. Reyes, E. Herrero, S. Casuscelli, G. Eimer, Top. Catal 54 (2011) 160–169.
[26] F. Gao, Y. Zhang, H. Wan, Y. Kon, X. Wu, L. Dong, B. Li, Y. Chen, Microp. Mesop. Mater 110 (2008) 508–516.
[27] B. Solsona, T. Blasco, J.M. López, M.L. Peña, F. Rey, A. Vidal-Moya, J. Catal. 203 (2001) 443–452.
[28] Y. Hu, S. Higashimoto, S. Takahashi, Y. Nagai, M. Anpo, Catal. Lett. 100 (2005) 35–37.
[29] C.W. Lee, W.J. Lee, Y.K. Park, S. Park, Catal. Today 61 (2000) 137–141.
[30] T. Sen, V. Ramaswamy, S. Ganaphaty, P. Rajamohanan, S. Sivasanker, J. Phys. Chem. 100 (1996) 3809–3817.
[31] G. Centi, S. Perathoner, F. Trifiro, A. Aboukais, C. Aissi, M. Guelton, J. Phys. Chem. 96 (1992) 2617–2629.
[32] M. Peña, A. Dejoz, V. Fornés, F. Rey, M. Vázquez, J. López Nieto, Appl. Catal. A 209 (2001) 155–164.
[33] K.J. Chao, C.N. Wu, H. Chang, J. Phys. Chem. B 101 (1997) 6341–6349.
[34] J. George, S. Shylesh, A. Singh, Appl. Catal. A 290 (2005) 148–158.
[35] Ch Subrahmanyama, B. Louisb, B. Viswanathana, A. Renkenb, T. Varadarajan, Appl. Catal. A 282 (2005) 67–71.
[36] M. Demeter, M. Neumann, W. Reicheit, Surf. Sci. 41 (2000) 454–456.
[37] B. Weckhuysen, D. Keller, Catal. Today 78 (2003) 25–46.
[38] D. Trong On, S. Nguyen, V. Hulea, E. Dumitriu, S. Kaliaguine, Micropor. Mesopor. Mater. 57 (2003) 169–180.
[39] D. Srinivas, R. Srivastava, P. Ratnasamy, Catal. Today 96 (2004) 127–133.
[40] B. Chakraborty, B. Viswanathan, Catal. Today 49 (1999) 253–260.
[41] A. Sakthivel, S. Dapurkar, N. Gupta, S. Kulshreshtha, P. Selvam, Micropor. Mesopor. Mater. 65 (2003) 177–187.
[42] T. Conesa, J. Hidalgo, R. Luque, J. Campelo, A. Romero, Appl. Catal. A 299 (2006) 224–234.
[43] C. Otero Areán, M. Rodríguez Delgado, V. Montouillout, J. Lavalley, C. Fernández, J. Cuart Pascual, J. Parra, Micropor. Mesopor. Mater 67 (2004) 259–269.
[44] L. Cedeño, D. Hernández, T. Klimova, J. Ramirez, Appl. Catal. A 241 (2003) 39–50.
[45] G. Turnes Palomino, J. Cuart Pascual, Rodríguez Delgado, M. Bernardo Parra, C. Otero Areán, Mater. Chem. Phys. 85 (2004) 145–148.
[46] E. Escalona Platero, M. Peñarroya Mentruit, C. Otero Areán, A. Zecchina, J. Catal. 162 (1996) 268–276.
[47] C. Morterra, G. Magnacca, Catal. Today 27 (1996) 497–532.
[48] L. Chen, L. Noreña, J. Navarrete, J. Wang, Mater. Chem. Phys. 97 (2006) 236–242.
[49] H. Kosslick, G. Lischke, G. Walther, W. Storek, A. Martin, R. Fricke, Micropor. Mater. 9 (1997) 13–33.
[50] A. Infantes-Molina, J. Mérida-Robles, P. Maireles-Torres, E. Finocchio, G. Busca, E. Rodríguez-Castellón, J.L.G. Fierro, A. Jiménez-López, Micropor. Mesopor. Mater. 75 (2004) 23–32.
[51] P. Van der Voort, M. White, M. Mitchell, E. Vansant, Spectrochim. A 53 (1997) 2181–2187.
[52] Y.M. Liu, Y. Cao, N. Yi, W.L. Feng, W.L. Dai, S.R. Yan, H.Y. He, K.N. Fan, J. Catal. 224 (2004) 417–428.